Numerical Simulations of Buoyant Ekman Layers. Part II: Rectification in Zero-Mean, Time-Dependent Forcing, and Feedback on the Interior Flow

ANASTASIA ROMANOU* AND GEORGES L. WEATHERLY

Department of Oceanography, The Florida State University, Tallahassee, Florida

(Manuscript received 2 July 2003, in final form 13 October 2003)

ABSTRACT

The response of the turbulent buoyant bottom Ekman layer near a temperature front over uniform topography is studied here. The background stratification is variable across the slope; the upper slope is either neutrally or stably stratified at one-half of the gradient of the lower slope region. In case 1, a time-dependent, spatially uniform, along-isobath interior current with zero mean causes residual circulation across the boundary layer and net detachment of the fluid from the boundary layer. For forcing with time scales longer than the shutdown time scale [$\tau_0 = f/(N\alpha)^2$; e.g., as defined by McCready and Rhines, where f is the Coriolis parameter, N is the Brunt–Väisälä frequency in the lower slope region, and α is the bottom slope], it is shown that the front represents an area of strong mean flow convergence and subsequent net detrainment of boundary layer fluid into the interior and is also a region of significant relative vorticity generation by the mean field. The residual circulation occurs in the stratified region. However, its direction and magnitude are subject to the order at which the downwelling and the upwelling phases occur because the lower and upper parts of the boundary layer respond differently to the two phases. The results are sensitive to the choice of background diffusivity. Tidal forcing produces significant differentiation in the results only when superimposed to the low-frequency current. The mean circulation then has much weaker downslope and along-slope components to the right of the front (i.e., seaward of the front). The strength of the detrainment at the front is found to be the same as in the low-frequency forcing case. In case 2, constant southward current causes convergence in the boundary layer, upwelling into the interior, vertical displacement of the isopycnals, and, through the thermal wind balance, a southward jet in the interior. This jet, which is the result of boundary layer dynamics and the presence of a front, could relate and explain the shelfbreak jet. As is shown here, a possible mechanism for the formation of an along-isobath jet (not just a shelfbreak jet) is the convergence in the bottom boundary layer, which, according to buoyant Ekman layer theory, may occur in the presence of one at least of the following: a front that intersects the bottom of constant inclination or constant stratification and a shelfbreak.

1. Introduction

The evolution of the buoyant bottom Ekman layer around a temperature front under constant interior forcing has been addressed in several papers (Romanou and Weatherly 2001, hereinafter RW-I; Chapman and Lentz 1994; and Chapman 2000). The first part of the present study is an extension of RW-I. Unlike in other studies, a time-dependent interior current with zero mean is considered here. In the second part of the study, a stably stratified upper-slope region and a constant interior current, similar to Chapman and Lentz (1994) and Chapman (2000), are studied.

The effect of the temporal variability of the interior current on the bottom boundary layer (BBL) flow has been discussed by various authors. Weatherly (1975) studied numerically the diurnal tide with no-zero mean in the presence of stratification and over both a level and a sloping boundary. Some of the important characteristics of the time-dependent turbulent Ekman layers were described: the hysteresis effect, that is, the fact that because of friction the bottom currents in the BBL are out of phase and essentially lead over the interior driving currents, the presence of transients (inertial oscillations), and the lack of repeatability over different tidal cycles because of their effect. The formulation of the BBL height under nonstationary conditions was tested and found to be in reasonable agreement with observations from the Straits of Florida.

In a subsequent paper, Weatherly et al. (1980) proposed a technique for the calculation of the BBL height and the bottom stress. The interior driving current was decomposed into a steady flow and two polarized tidal currents (clockwise and counterclockwise). It was shown that the clockwise tidal current with frequency comparable to the local Coriolis parameter creates thicker boundary layers and the bottom drag is increased.

* Current affiliation: Courant Institute of Mathematical Sciences, New York University, New York, New York.

Corresponding author address: Dr. Anastasia Romanou, Columbia University, 2880 Broadway, New York, NY 10025.
E-mail: ar2235@columbia.edu

Richards (1982) also studied the effect of tidal forcing in the benthic boundary layer using a numerical model with a second-order turbulence closure scheme. Both a neutrally and a stably stratified ocean over a flat boundary were considered and a phase shift between the shear and the stress was observed. The author suggested that rapid distortion effects are responsible for the hysteresis since the typical turbulence time scale is much greater than the interior forcing time scale. The phase shift was found to reduce the production of turbulence significantly. He also found that the growth rate of the bottom mixed layer (BML) height is 30% less under tidal forcing than under a constant interior current of the same magnitude.

The importance of using time-dependent eddy viscosity models to study the tidally and inertially driven boundary layer flows was pointed out by McLean and Yean (1987). Using a one-dimensional, time-dependent model and comparing the results to deep ocean observations, they predicted increased boundary layer velocities and stresses and argued that, if the mixed layer is thinner than the boundary layer, shear is introduced at the top of the boundary layer.

Furthermore, observations from the northern California shelf suggest that the BML height decreases when the interior current is such that the Ekman transport is upslope. Lentz and Trowbridge (1991) attributed the the thinning of the mixed layer to the upslope advection of colder water during upwelling.

The response to a low frequency and to a tidal interior flow were examined numerically by Ramsden (1995). He used a one-dimensional model in which the eddy viscosities and diffusivities depended on a gradient Richardson number criterion. The BML height and the mixing rate were found to depend on the interior boundary condition, that is, on whether a pressure forcing was present. In the low-frequency-forcing case, the Ekman flow was arrested during both parts of the forcing cycle, and the mixed layer height evolution was in agreement with observations. In the tidal case, net upslope flow and weak average mixing rates were predicted.

The one-dimensional numerical description of the BBL evolution under time dependent forcing using the Mellor–Yamada level-2 closure scheme (Middleton and Ramsden 1996) showed that the BBL height continues to grow during the downwelling deceleration phase and that the cross-slope velocity and stress component lead over the interior current. The authors attributed the phase difference to the thermal-wind shear that is maintained at the top of the boundary layer. During the upwelling deceleration phase, the bottom stress and the boundary layer height decreased and at the end of the cycle a net upslope flow of 0.5 cm s^{-1} was established. Residual along-slope flows were not considered.

Several authors (Pickart 2000; Chapman 2000; Fratantoni et al. 2001; Lozier and Gawarkiewicz 2001) have described the shelfbreak jet in the Middle Atlantic Bight associated with the existence of the shelfbreak front. Pickart (2000) looked at detailed hydrographic measurements near a shelf break for the PRIMER experiment area. He found that the density front was centered at 90 km from the coast, 40 km farther upslope (to the left) of the shelf break. In fact, another drop in the topography at 100 km from the coast was actually closer to the front. The author also used an advective–diffusive model to explain the jet. Implications of BBL dynamics in the formation of the jet could not be made because there were the observations of the hydrographic structure of the BBL only extended to 3–5 m above the bottom.

Chapman (2000) studied the offshore displacement of the Middle Atlantic Bight front. He found [as did Gawarkiewicz and Chapman (1992), Chapman and Lentz (1994), and Yankofsky and Chapman (1997) earlier] that both the along-slope and the cross-slope evolution of the boundary layer need to be taken into account for the formation and maintenance of the front. As in RW-I, the convergence at the bottom boundary layer caused the flow to leave the BBL and move upward. However, in all the above studies (except in RW-I) the final position of the front on the slope, which was caused by the inhibition of the bottom Ekman flow, was not necessarily related to the shelf break. The front stopped migrating farther offshore at a depth $h = (2Mf\rho_0/g')^{1/2}$, where M is the transport of the front, f is the Coriolis parameter, ρ_0 is the ambient density, and g' is the reduced gravity describing the front (Yankofsky and Chapman 1997). Chapman (2000) showed that this depth is much shallower if there is background stratification. However, although Chapman (2000) demonstrates very successfully the effect of BBL dynamics on the front migration, its final location is not the shelf break. In the present study, and in the discussion section, it is shown that BBL dynamics may create a shelfbreak front.

Fratantoni et al. (2001) described the structure and dynamics of the shelfbreak jet during autumn and winter, showing that to first order it is a geostrophic current. Lozier and Gawarkiewicz (2001) described the structure and cross-stream exchanges of the shelfbreak jet using surface drifters and found that it is a robust feature along the Middle Atlantic Bight from Georges Bank southward to Cape Hatteras.

The present paper is organized as follows: The theoretical framework and a brief description of the model used are given in sections 2 and 3, respectively. In section 4, the results of an ensemble of model runs are presented. In section 4a a time-dependent, low-frequency interior current, a constant bottom slope, a neutrally stratified upper slope, and a stably stratified lower slope are considered. The sensitivity of the results of the standard case [section 4a(1)] are tested under variation of controlling parameters such as an extended forcing cycle [section 4a(2)], a reversed forcing cycle [section 4a(3)], increased background diffusivity [section 4a(4)], and increased bottom inclination [section

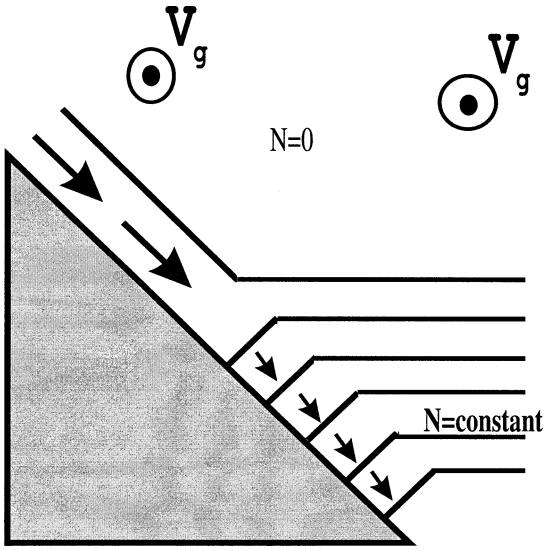

FIG. 1. Schematic representation of the low-frequency-forcing case. Boundary layer formed over bottom with constant slope and varying interior stratification. The time-dependent interior current V_g flows along the isobaths (i.e., in the y direction), and the Coriolis parameter f is positive. The temperature jump above the BBL in the upper-slope region limits the BBL thickening and is similar to the BBL over a level bottom while the BBL in the stratified region is a buoyant BBL.

4a(5)]. In section 4b a constant interior current, a stably stratified upper slope, and twice as much stratified lower slope are considered, and the effect of the boundary layer dynamics to the interior current is discussed.

2. Methodology

a. Model domain

In the first part of the present study, and following RW-I, the upper part of the study area is almost neutrally stratified (Fig. 1). A small temperature jump is initially inserted 5 m above the bottom to limit the BBL thickening. The BBL in this region is essentially the same as that above a level bottom. The lower part of the study area (Fig. 1) is uniformly stratified with level isotherms (isopycnals) in the interior. The interior current is uniform, flowing along the isobaths, and its magnitude varies with time.

In the second part, the upper slope is also stably stratified at one-half of the stratification of the lower-slope region. In this case, the interior current is flowing along isobaths but its magnitude is constant.

b. Governing equations

Following RW-I, the momentum equations for a Boussinesq, rotating stratified ocean in a bottom embedded coordinate system are

$$u_t + \mathbf{u}\cdot\nabla u - fv = -p_x + g\beta\alpha(T - \overline{T}) + (A^x u_x)_x + (A^z u_z)_z \quad (1)$$

and

$$v_t + \mathbf{u}\cdot\nabla v + fu = (A^x v_x)_x + (A^z v_z)_z, \quad (2)$$

where the x axis points downslope across the isobaths and $x = 0$ is the location of the front initially. The z axis is perpendicular to the bottom boundary and the bottom slope α is assumed small so that $\sin\alpha \approx \alpha$ and $\cos\alpha \approx 1$. Only terms greater or equal to $O(\alpha)$ are retained; the interior velocity $V_g = p_x/(\rho f)$ is uniform along the slope and so is $\overline{T}$, the background temperature field. A linear equation of state is assumed, that is, the density variations result from temperature changes only, $\rho/\rho_0 = (1 - \beta T)$, where β is the thermal expansion coefficient; $A^{x,z}$ are the eddy viscosities.

The density and continuity equations maintain their form in the rotated coordinate system:

$$T_t + uT_x + wT_z = (K^x T_x)_x + (K^z T_z)_z \quad (3)$$

and

$$u_x + w_z = 0, \quad (4)$$

where $K^{x,z}$ are the eddy diffusivities for heat.

c. Boundary and initial conditions

To close the problem, the following boundary conditions need to be employed. At the bottom ($z = 0$), there is the slip condition,

$$u = v = 0, \quad (5)$$

and the insulated bottom,

$$T_z = 0, \quad (6)$$

that is, no heat flux through the bottom. The kinematic bottom boundary condition is ensured by parameterizing the logarithmic layer in the BBL.

At the top of the domain, well outside the bottom boundary layer; that is, as $z \to \infty$,

$$p_x = fV_g \quad \text{and} \quad (7)$$

$$T_z = 0. \quad (8)$$

The top boundary is considered to be thermally insulated and the side boundaries are perfect conductors of momentum and heat.

d. Parameters and scaling

In the first part of the study, the pressure gradient at the top of the model (p_x, p_y) is set to $(fV_g, 0)$, where $V_g = V_0 \sin\omega t$ and $V_0 = \pm 15$ cm s^{-1}. The background stratification $\overline{T}_z = 7 \times 10^{-4}$°C cm^{-1}, and the interior Brunt–Väisälä frequency $N = 1.28 \times 10^{-2}$ s^{-1}. The bottom slope is $\alpha = 2.4 \times 10^{-3}$, the thermal expansion coefficient is $\beta = 2.4 \times 10^{-4}$ °C^{-1}, and the Coriolis parameter is $f = 6.3 \times 10^{-5}$ s^{-1}.

In the second part of the study, the parameters are

kept the same except that the upper half of the domain is also stably stratified at $\overline{T}_z = 3.5 \times 10^{-4}$ °C cm^{-1} and the geostrophic current is constant $V_g = V_0 = -15$ cm s^{-1}.

In the following, positive (negative) y direction or flow with shallow water on the left (right) will be related for simplicity, albeit not precise, to the notion of north (south). The background vertical eddy viscosity and the eddy diffusivity are $A_0^z = 10^{-2}$ cm^2 s^{-1} and $K_0^z = 10^{-3}$ cm^2 s^{-1}, respectively. The parameterization is chosen to facilitate comparison with Middleton and Ramsden (1996).

For this problem (and as in RW-I), the McCready and Rhines (1993) time scale,

$$\tau_0 = f/(N\alpha)^2 = 18.5 \text{ h}, \quad (9)$$

is the time for the buoyancy terms in Eq. (1) to become the same order of magnitude as the Coriolis and turbulence terms. In the first part of the paper, over the lower slope region, the characteristic time scale of the flow is $\tau = 2\pi\omega^{-1} \gg \tau_0$. Therefore the BBL Ekman flow will be arrested by buoyancy there, while on the upper region the Ekman flow is not arrested. In the second part, the characteristic time scale of the flow is larger than the McCready and Rhines (1993) time scale in both the upper and the lower slope; therefore, the Ekman flow is arrested in both regions.

3. The numerical model

The model used in the following simulations is the three-dimensional primitive equation Sandia Ocean Modeling System (SOMS-3D), developed by Dietrich et al. (1987) and Dietrich (1993). An initial surface mixed layer 5 m deep is assumed everywhere across the slope. In the first part of the paper, above the upper slope a steplike temperature jump at $z = 5$ m is assumed so as to limit the BBL thickening there. Basically the boundary layer in that region is similar to that over a level bottom boundary capped by a temperature jump (Weatherly and Martin 1978). In the second part of the paper, both upper and lower slope are stratified and the initial BML height is 5 m.

The domain is $L = 160$ km wide across and along the slope and the depth $H = 100$ m. The grid spacing is $\delta x = 2$ km and $\delta y = 50$ km. Sensitivity runs with $\delta x = 500$ m show that the results were nearly insensitive to the resolution (some discussion will be given in the last section). The bottom is assumed hydrodynamically rough and the roughness length scale z_0 is taken as constant, $z_0 = 3 \times 10^{-2}$ cm. The vertical grid is stretched, being logarithmic close to the bottom and linear in the interior. There are four levels within the first 5 m while in the interior $dz \approx 3$ m. The time step, $\delta t = 20$ min, is chosen to satisfy the Courant stability criterion $C(\delta t/\delta x) \ll 1$, where C is the speed of the fastest-moving internal wave. For the higher-resolution runs the time step is decreased to 1 min.

The horizontal diffusivities are modeled according to Yamada (1979), with the background diffusion of momentum and heat equal to 10^{-1} and 5×10^{-2} cm^2 s^{-1}, respectively. The Mellor–Yamada 2½-order turbulence closure scheme (1982) is used for the calculation of the vertical eddy viscosity and diffusivity. To ensure the no-slip boundary condition at the bottom, the logarithmic ''law of the wall'' is applied at the lowest vertical grid levels. To eliminate the static instabilities, the Mellor–Yamada scheme is implemented with a convective adjustment scheme that instantaneously (i.e., at every time step) mixes any unstable regions. Further details on the numerical scheme can be found in RW-I.

4. Results

a. Low-frequency interior current with neutrally stratified upper slope and uniformly stratified lower slope

1) LOW BACKGROUND DIFFUSION

In general the oceanic interior currents are time dependent and with a wide range of frequencies. One low-frequency variability with a period of about 23 days, observed in the Cape Hatteras shelfbreak region (Kim et al. 2001), is considered here. The interior along-isobath current varies in time as $V_g = V_0 \sin\omega t$, where $\omega = 2\pi/23$ days $= 3.2 \times 10^{-6}$ s^{-1} and $V_0 = 15$ cm s^{-1}. The upper slope is nearly neutrally stratified and the lower slope region is uniformly stratified. In the following, this experiment will be referred to as the ''standard case.''

During the first half of the cycle (upwelling phase), the northward interior current effects an upslope Ekman flow; during the second half (downwelling phase), the southward current causes reversal of the flow in the Ekman layer as well. Since the shutdown time scale [Eq. (9)] is much less than the period of the flow ($\tau_0 \ll \tau = 2\pi\omega^{-1}$) and as Middleton and Ramsden (1996) suggested, the buoyancy term in Eq. (1) becomes important inside the BBL over the lower slope throughout the forcing cycle.

In the lower slope region for the first quarter of the cycle, when the current is accelerating northward and an upwelling Ekman flux is established inside the boundary layer, turbulence is inhibited and the mixed layer collapses (Figs. 2c,d). The BBL current leads the interior current [as in Weatherly (1975) and Richards (1982)]. Middleton and Ramsden (1996) noted that this phase shift is strongly affected by the thermal wind effects in the BBL. The stratification inside the BBL is reduced toward the end of the second quarter. Before the cycle is completed there is upwelling close to the boundary due to the phase shift and the lower part of the mixed layer restratifies.

This behavior is extended to the area immediately around the front. During the first half of the cycle, upwelling leads to the collapse of the mixed layer at 2 km

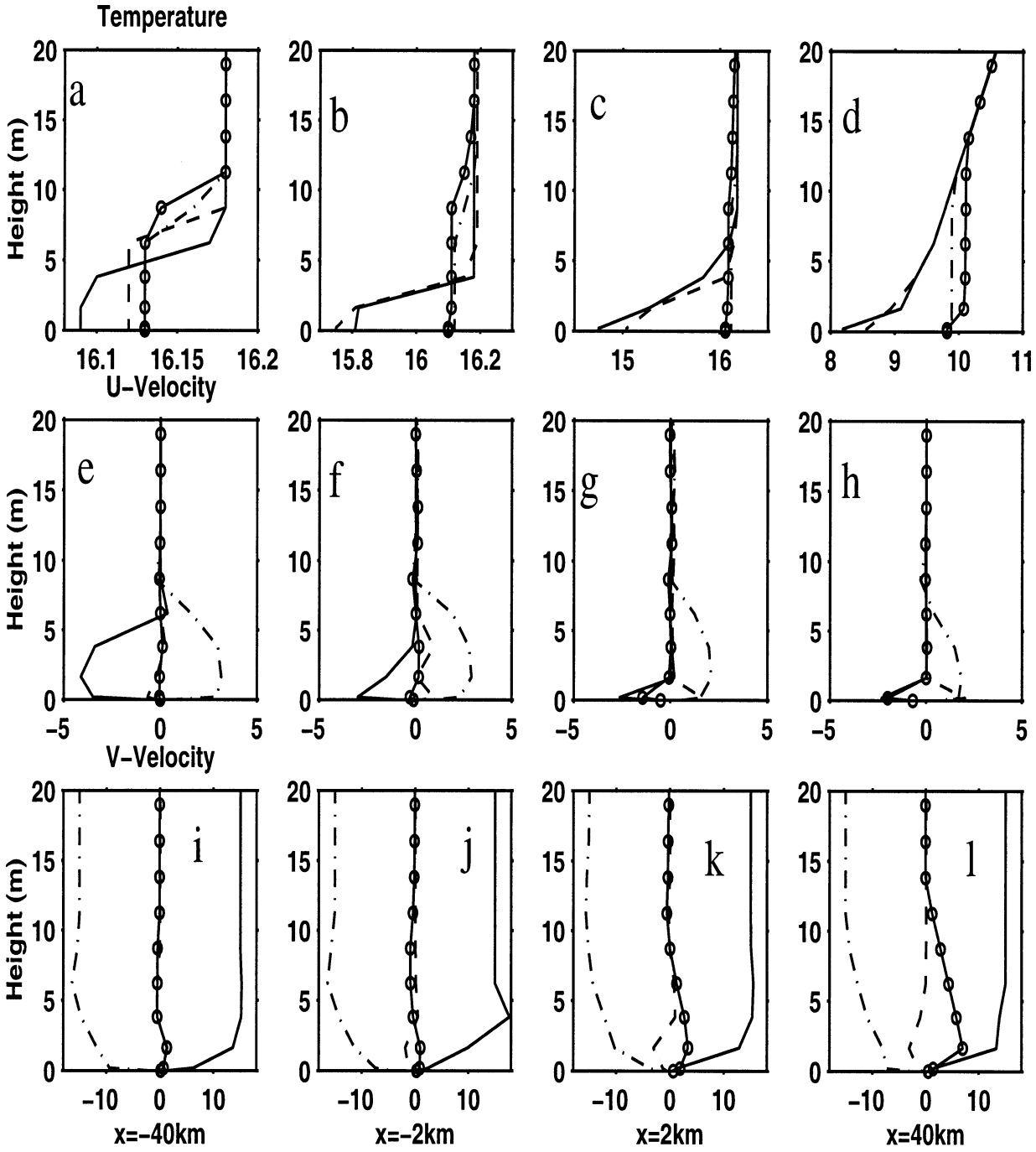

FIG. 2. Low-frequency forcing: vertical profiles *upslope* (first column), *before* the front (second column), *after* the front (third column), and *downslope* (last column) of temperature (°C), cross-slope velocity u (cm s^{-1}), and along-slope velocity v (cm s^{-1}) at one-quarter cycle (continuous line), one-half cycle (dashed line), three-quarters cycle (dashed dotted line), and end of cycle (continuous line with circles). Labels at the bottom of each column indicate the cross-slope displacement relative to the initial position of the front.

to the left of the front but not as much as at 2 km to the right of the front or farther downslope (Figs. 2b,c,d). The velocity profiles to the left of the front show that the flow there is little affected by the shutdown processes on the lower slope (Figs. 2f,j).

During the second half of the cycle (downwelling), the boundary layer over the lower slope remixes quickly to 6 m during the accelerating quarter and to 8 m by the end of the cycle. Both u and v have the same structure as at the upper slope region, except during the last quarter where upwelling is still observed. To the right of the front (Figs. 2c,g,k) the mixed layer collapses

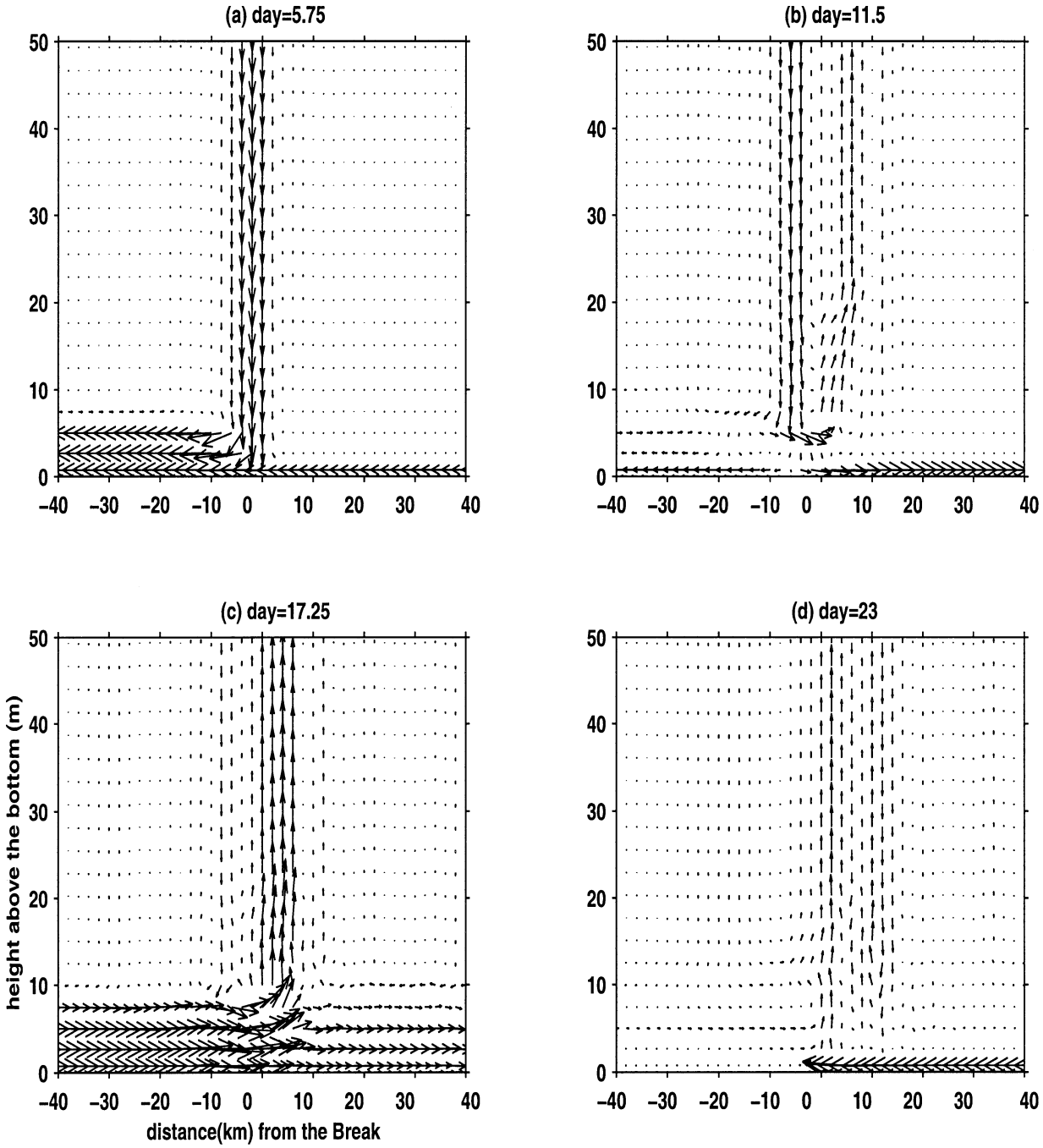

FIG. 3. Low-frequency forcing: cross-slope sections of the u, w velocity (cm s^{-1}) at each quarter period.

during the first quarter and by the end of the second one it has started restratifying. The average cooling and subsequent warming of the column are less than in the stratified region.

More concisely the circulation across the slope in the (x, z) plane is shown in Fig. 3. At the end of the first quarter the flow is everywhere upslope, but stronger in the upper half of the domain. Therefore, downwelling is induced at the center of the domain (Fig. 3a). By the end of the first half of the interior forcing period the flow in the BBL is reduced and finally changes direction (now downslope) (Fig. 3b). For the remaining time the flow increases in magnitude and is directed downslope in the upper region, inducing upwelling in the middle of the domain (Fig. 3c). By the end of the cycle the flow in the BBL has already switched direction and now flows upslope (Fig. 3d).

There is a net circulation at different levels in the

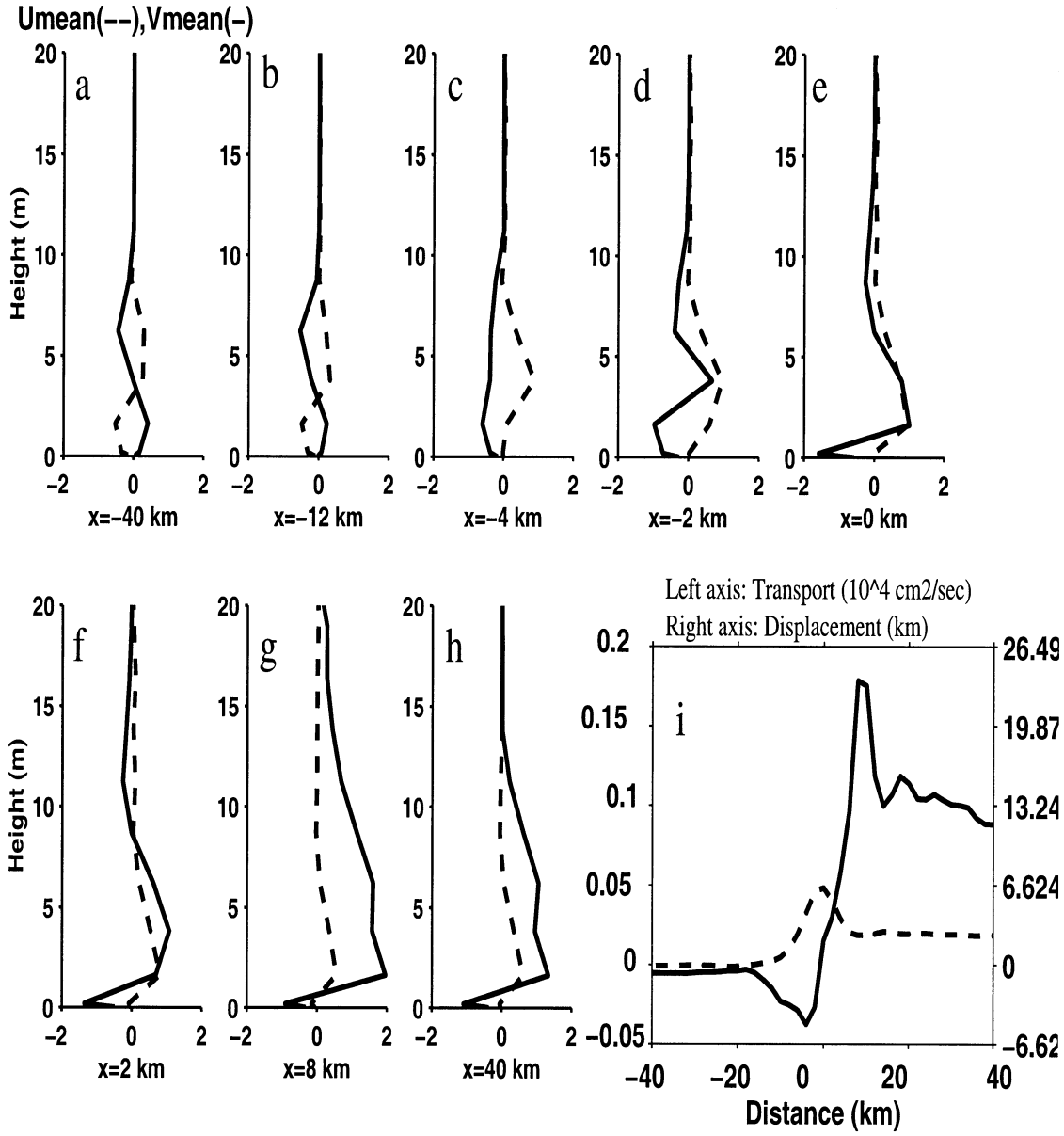

FIG. 4. Low-frequency forcing: (a)–(h) mean cross-slope (dashed line) and along-slope (continuous line) velocity profiles (cm s^{-1}) over one cycle (23 days) at various positions downslope. The positions downslope are shown at the bottom of each plot and represent the distance (km) from the front (at $x = 0$ km). (i) Vertical integrals of the profiles shown in (a)–(h) of this figure represent net transports ($\times 10^4$ cm^2 s^{-1}; left axis) across (dashed line) and along (continuous line) the bottom boundary. The right axis shows the displacements (km), which is the depth-averaged mean velocity for the entire time period.

BBL everywhere across the slope. However, this rectified flow at the top of the slope (Fig. 4a) is an artifice, partly of the BBL thickening during the last half of the cycle and partly of the hysteresis effect. Note that, as expected, the BBL transports are very nearly zero there (Fig. 4i). Close to the front (Figs. 4b–d), the mean flow turns increasingly downslope and to the south throughout the boundary layer. At 5 m above the bottom at the front, the alongslope flow reverses direction and flows northward, with its magnitude increasing farther downslope. Therefore, the front is both an area of mean cross-slope flow convergence and of mean vorticity, v_x, generation.

Net downslope circulation is expected at the upper levels of the BBL in the stratified region. This can be justified as follows. In Fig. 2h, the BML is 10 m thick during the downwelling phase and only 2 m during the upwelling phase. Therefore between 2 and 10 m above the bottom, there is a net cross-isobath flow (downslope). However, in the lower BBL there is both upslope and downslope motion during the cycle, the relative strength of each depending on the choice of background

diffusion (RW-I; Middleton and Ramsden 1996). For low (i.e., molecular) background diffusion there is net downslope circulation in the lower BBL (Fig. 2h). However, for high background diffusion (1 $cm^2\ s^{-1}$) there is upslope transport in the lower BBL (Middleton and Ramsden 1996; Romanou 1999, her Fig. 5.25).

By the end of the cycle the along-slope circulation to the right of the front is to the north throughout the boundary layer (Fig. 2l) because the linear profile at the top of the downwelling boundary layer (above 2 m) reduces v faster than during the upwelling phase where v is positive. At the same time v leads the forcing and that imposes a northward circulation at the end of the downwelling phase and within a boundary layer 12 m thick. The net effect is a northward transport (Fig. 4i).

Upslope of the front the net displacement of the fluid particles inside the BBL (vertical integral of the profiles in Figs. 4a–h) is negligible. However, over the lower slope the net displacements are 4 km downslope and 11 km to the north. The most extreme downslope displacement, almost 8 km, occurs at the front because during downwelling u there is larger than farther downslope. During upwelling the area to the right of the front experiences the intrusion of cold and slow slope water (Fig. 2f). The mean along-slope displacement is almost 8 km to the south to the left of the front and 23 km to the north to the right of the front.

In RW-I it was shown that during upwelling Ekman flow divergence around the front entrains interior fluid toward the boundary layer, and during downwelling Ekman flow divergence detrains boundary fluid into the interior. As in RW-I Fig. 13a, passive tracer (dye) is injected over the lower half of the slope and its initial concentration is uniform up to 5 m above the bottom. Subsequently and since the divergence/entrainment (Figs. 5a,b) and the convergence/detrainment (Figs. 5c,d) occur at different positions downslope and have different magnitudes, there is eventually a net effect in the interior. Thus, at the end of the cycle (Fig. 5d) tracer is detrained from the BBL around the front to 40 m in the interior. Further, tracer on the slope is advected 10 km upslope by the end of the first quarter (Fig. 5a), 18 km by the end of the second (Fig. 5b), and by the end of the cycle it has retreated to almost 6 km (Fig. 5d).

2) A SECOND CYCLE

During a second cycle with the same interior forcing, the profiles over the upper slope change little. Farther downslope the temperature profile is quite different at the beginning of the second cycle (Fig. 5d) than it was at the beginning of the first cycle. The BBL velocity field is not zero at the beginning of the second cycle, and therefore during the upwelling phase only the lowest part of the BML restratifies. The rest remains almost unaffected. Such staircase-like layers were observed by Lentz and Trowbridge (1991) offshore on the north California shelf and have been modeled with an upwelling phase following a downwelling one by Middleton and Ramsden (1996).

As expected, the two cycles are very similar only in the upper slope. However, the asymmetry between the upwelling and downwelling parts of the first cycle, as well as the fact that the fluid column does not respond in-phase with the interior current (because of the hysteresis effect), impose a net circulation as initial condition for the second cycle. The focus of the present study is how such staircase like layers affect the region around a front.

Unlike the first cycle, the BBL ejects fluid toward the interior during both the upwelling and downwelling phases, and by the end of the cycle tracer is found farther up in the interior (100 m above bottom Fig. 6) as compared with only 40 m at the end of the standard cycle. During upwelling (Figs. 6a,b) cold slope water extends to 15 km upslope to the left of the front; the mixed layer is very thin (about 1 m) and is capped by a strong stratification. The mixed layer to the left of the front is also modified to 30 km to the right of the front. During the downwelling phase (Figs. 6c,d) the mixed layer shows staircase-like form to the right and farther downslope from the front, and tracer is found up to 10 km to the left of the front.

3) REVERSED INTERIOR CURRENT

As the results of Middleton and Ramsden (1996) suggest, a cycle of interior forcing where the upwelling phase precedes the downwelling one [as in section 4a(1)] will result in a different BBL structure than when the downwelling phase occurs first. Moreover, the BBL flow adjustment during the second cycle of the interior current [section 4a(2)] was shown to create staircase-like mixed layers in the lower slope during upwelling. By reversing the direction of the interior current of section 4a(1), it will now be shown that these differences are the result of another kind of asymmetry, a phase asymmetry: the BBL response depends on the order in which the upwelling and the downwelling phases occur (i.e., which one comes first). The focus is again on the region around the front.

The reversal of the interior current does not greatly affect the detrainment of BBL flow and tracer toward the interior (as a comparison of Fig. 7 and Fig. 5 shows). By the end of the cycle there is again net detrainment, and tracer has reached 40 m in the interior. The BML at day 11.5 is very similar to the BML at day 23 in the standard case (Fig. 5d). The two BBLs however evolve very differently during the upwelling halves of the cycles. Staircase-like fronts develop in this case also, keeping the lower BBL to the right of the front less stratified (more mixing). By the end of the cycle more cold slope water has reached to 16 km upslope from the front (Fig. 7d). A larger area to the right of the front is affected (20 km vs 6 km in the standard case).

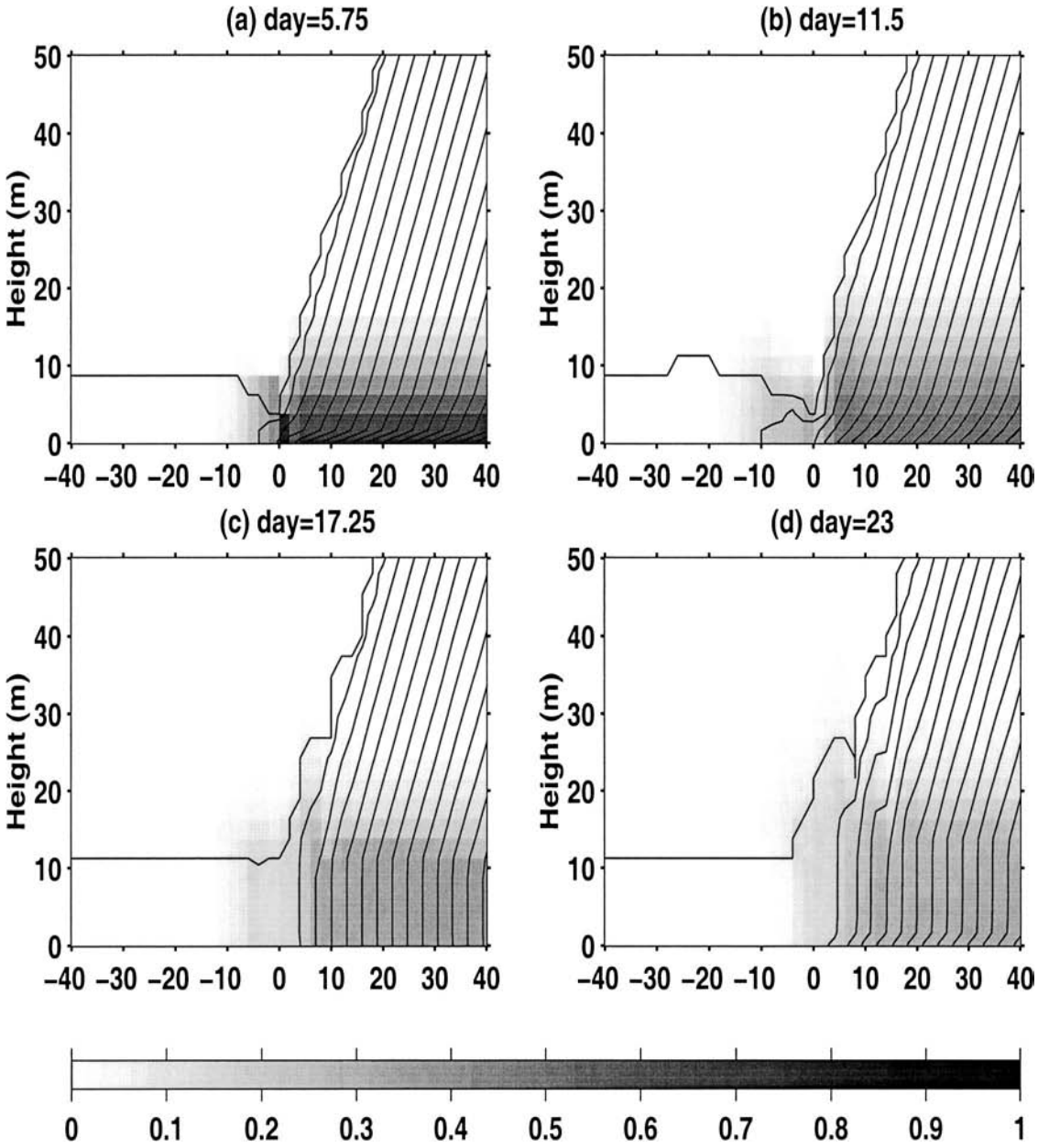

FIG. 5. Low-frequency forcing: passive tracer and temperature (°C) sections across the bottom boundary at the end of each quarter cycle. The horizontal axis is the distance from the initial position of the front (at $x = 0$ km). Tracer concentration legend is also shown. Isotherm contour interval = 0.5°C; max temperature = 16.18°C.

4) HIGH BACKGROUND DIFFUSION

In RW-I and Middleton and Ramsden (1996), increasing the background diffusivities to $A_0^x = K_0^x = 1$ cm^2 s^{-1} was shown to affect the BBL in the stratified region greatly. The effect of eddy rather than molecular background diffusivities to the BBL around the front is explored here.

Far to the right of the front the mean circulation (Fig. 8a) is directed to the north, as in the standard case [section 4a(1)], and upslope, unlike the standard case. In fact, the current there is weaker at the end of the downwelling phase than at the end of the upwelling phase, unlike the low-diffusion case but consistent with the stronger arrest of the downwelling Ekman flow in the high-background-diffusion case [discussed in RW-I and sections 4a(2) and 4b(2)]. The net displacement over one cycle is 2 km upslope and 7 km to the north (Fig. 8a) as opposed to 4 km downslope and 11 km to the north in the standard case (Fig. 4i).

Around the front the transport is in the same direction as in the standard case. To the left of the front the

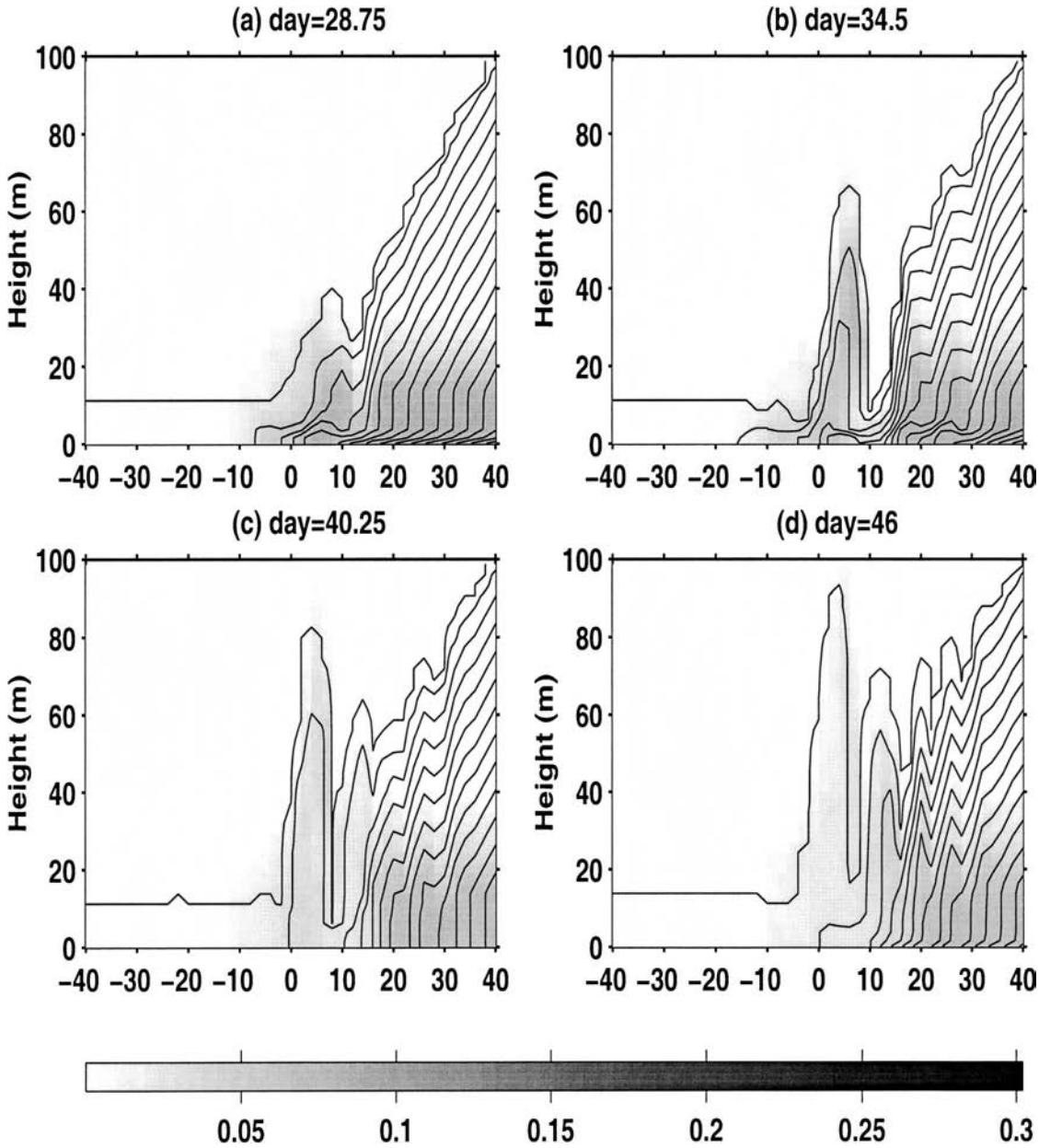

FIG. 6. Second cycle: as in Fig. 5, passive tracer and temperature (°C) sections across the slope at the end of each quarter cycle. Isotherm contour interval = 0.5°C; max temperature = 16.18°C.

displacement is 7 km (8 km) downslope and 26 km (8 km) to the south, while to the right of the front the displacement is 5 km upslope and 30 km (23 km) to the north (in parentheses are the respective values for the standard case). Again, the region of the front is an area of strong cross-slope velocity divergence and along-slope vorticity input (Romanou 1999).

5) STEEPER SLOPE

In RW-I, increasing the inclination of the slope region to 7.2×10^{-3}, that is, 3 times that in the standard case, led to a faster arrest of the Ekman flow in the stratified region. Also, the area around the front that became affected was narrower.

Here, over the lower slope the mean cross-slope component is essentially zero because of the stronger shutdown of the Ekman flow there (Fig. 8b). The along-slope displacement, however, is greater than in the standard case (20 km northward).

To the left of the front the maximum downslope displacement is 3 km and the maximum along-slope displacement is 7 km to the south. To the right of the front the mean displacement is almost 40 km to the north.

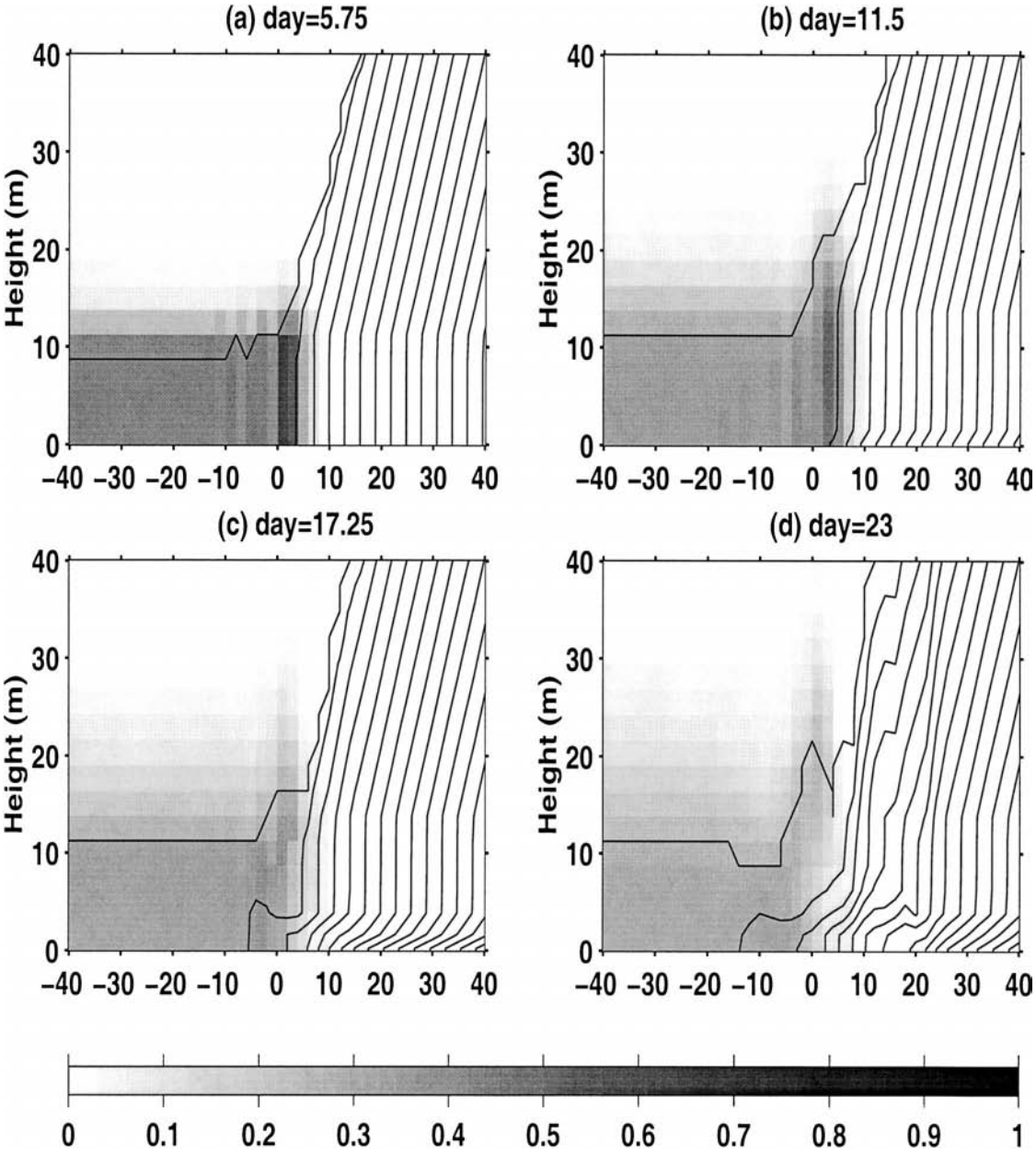

FIG. 7. Reversed interior current: as in Figs. 5 and 6, passive tracer and temperature (°C) sections across the bottom boundary at the end of each quarter cycle. Isotherm contour interval = 0.5°C; max temperature = 16.18°C.

Over the upper slope, far to the left of the front, the upslope net motion in the BBL is consistent with the steep-slope results of RW-I, where it was noted that during upwelling (downwelling) the upper-slope (lower-slope) BBL stress and transport were stronger (weaker). This was attributed to appreciable entrainment of surrounding interior fluid into the vertical flow ''column'' at the front. This effect is not noticeable in the standard run because there the flow column is not as narrow, and therefore the entrainment transport not as pronounced. The entrainment affects the transport to the left of the front only when the column is downward and discharges into the BBL there.

That the above noted asymmetry should also result in a rectified southward alongslope transport on the BBL to the left of the front can be seen by integrating Eq. (1b) of RW-I across the BBL:

$$\int_0^h \int_0^T v \, dt \, dz = \frac{1}{f} \int_0^T \tau^x(z_0) \, dt, \qquad (10)$$

where h is the BBL height, $T = 2\pi\omega^{-1} = 23$ days is a forcing cycle, and $\tau^x(z_0)$ is the bottom stress in the x

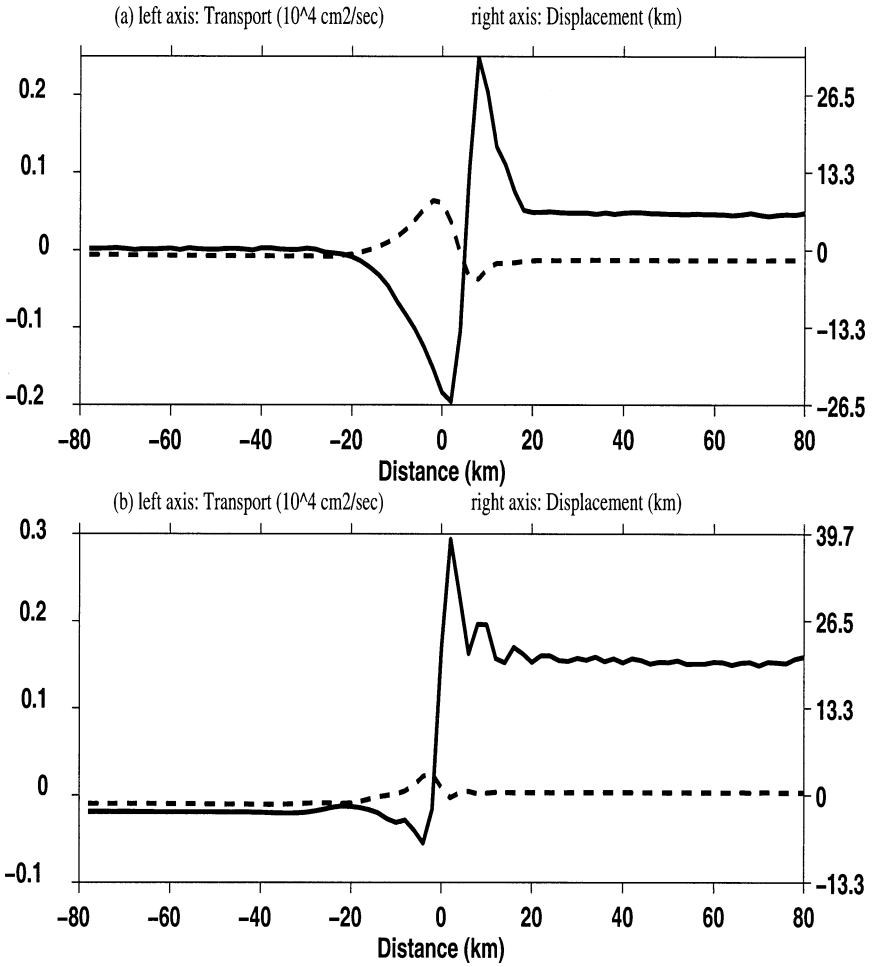

FIG. 8. Transports ($\times 10^4$ cm^2 s^{-1}; left axis) across (dashed line) and along (continuous line) the boundary. (a) Low-frequency forcing with high background diffusion and (b) low-frequency forcing over steeper slope. The right axis shows the displacements (km), which is the depth-averaged mean velocity for the entire time period.

direction. Because of the asymmetry in the cross-slope transport,

$$\int_0^{T/2} |\tau^x(z_0)|\, dt > \int_{T/2}^{T} |\tau^x(z_0)|\, dt,$$

and the right-hand side of Eq. (10) is negative, that is, there should be a net southward BBL transport.

6) TIDALLY MODULATED LOW-FREQUENCY INTERIOR CURRENT

In this section, the effect of higher-frequency forcing (nearly tidal) is explored. Tides, ubiquitous in the ocean, sometimes are the dominant variability on the continental shelf and slope, and substantial research has focused on their effect at these areas.

Middleton and Ramsden (1996) studied the BBL structure and evolution over the continental slope under tidal forcing. They found that there was essentially zero rectification and essentially no net transport across the slope due to the tides. Several assumptions that were made in their study, as well as in the present one, must be taken into account when comparing with observations: the model geometry was simplified, no along-slope variability was allowed, and in one case only purely tidal forcing was considered. In nature, along-slope flow evolution and interaction with flows with longer time scales may explain why tidal rectification is important in other continental shelves areas, for example, Georges Bank.

Under pure tidal forcing in the experimental set up of the standard case, Romanou (1999) also showed that the buoyancy effects never become important in the stratified region of the slope. The buoyancy field changes only because of the background diffusion. No arrested Ekman layer develops in the stratified region [in accordance with Middleton and Ramsden's (1996) results], and thus no detrainment/entrainment occurs around the front. This is because the shutdown time scale is $\tau_0 =$

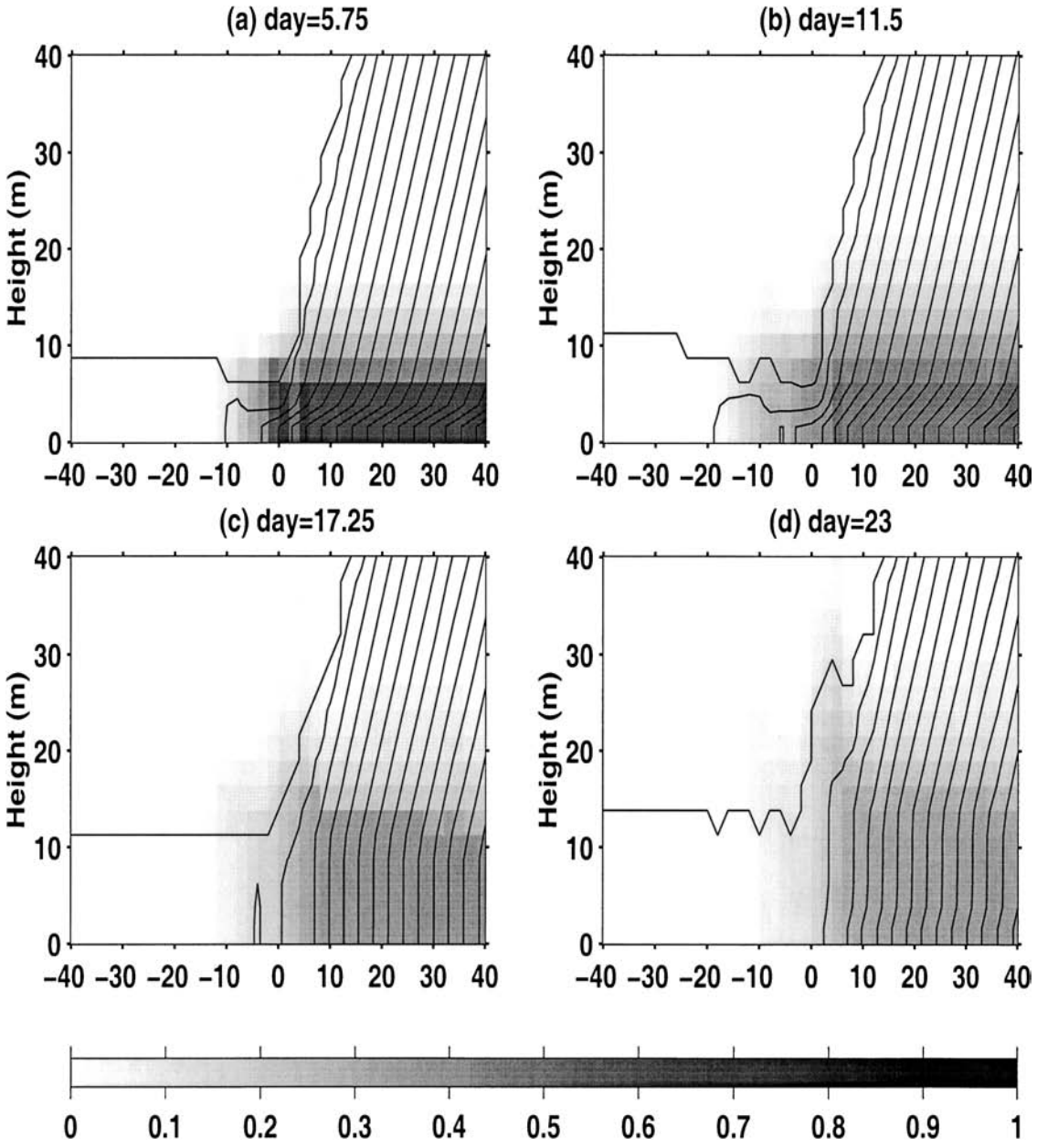

FIG. 9. Tidally modified low-frequency current: passive tracer and temperature (°C) sections across the bottom boundary at the end of each quarter cycle. Isotherm contour interval = 0.5°C; max temperature = 16.18°C.

18.54 h and the natural time scale of the flow is of the same order of magnitude as the shutdown time scale; that is, $\tau_0 \geq \tau = \pi\omega^{-1}$.

In this section, the combined effect of a low-frequency interior flow [as in section 4a(1)] and a superimposed tidal oscillation with amplitude $V_0^T = 8$ cm s^{-1} is described. The interior current is then $V = V_0 \sin\omega t + V_0^T \sin\omega_T t$.

The convergence and detrainment around the front due to the tide do not result in more effective detrainment of BBL fluid into the interior (Fig. 9). In both cases, by day 23, tracer is ejected up to 40 m in the interior. However, ejection of tracer in the interior occurs all along during this cycle and not only during the downwelling second half of the cycle, as in the standard case. Also, tracer reaches farther upslope from the front (to 10 km) than in the standard case (6 km).

The intrusion of cold lower-slope water to the area left of the front, which occurs during the first half of the cycle (note day 11.5 in Fig. 5b and Fig. 9b), extends to greater distances also (20 km here than 10 km in the standard case). The mixed layer over the lower slope does not collapse completely at the end of each quarter, which is an indication that some mixing is maintained

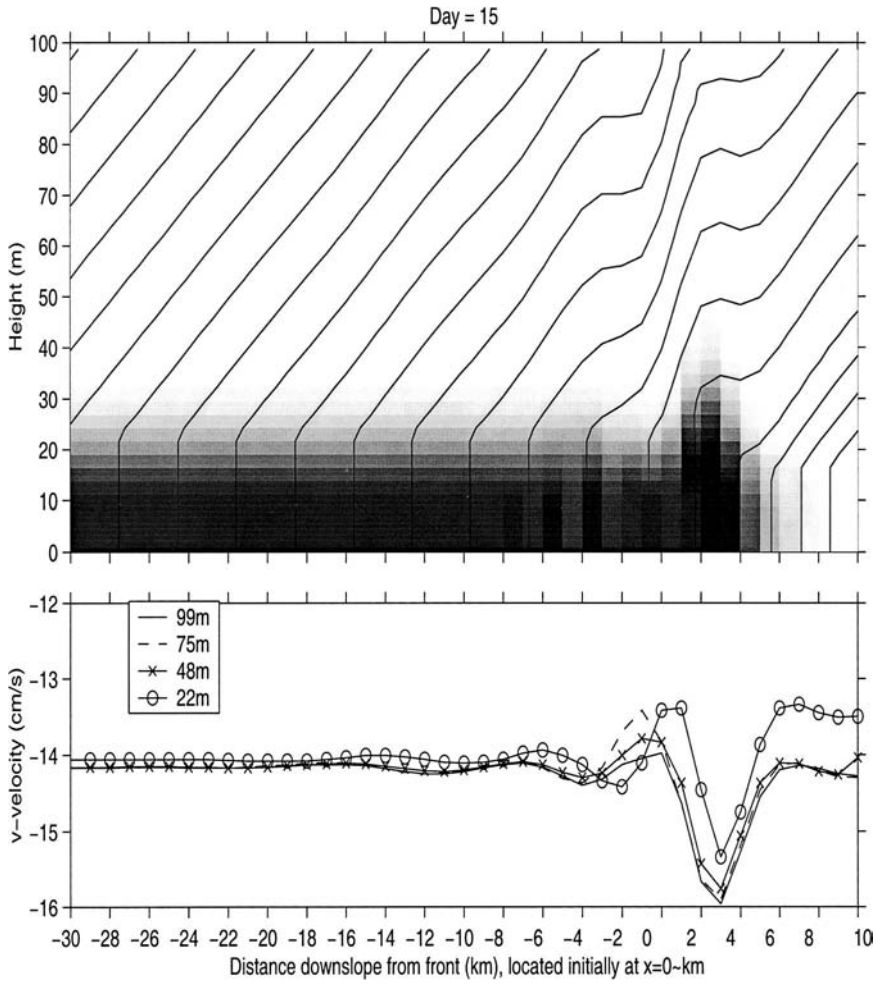

FIG. 10. Stratified upper slope: (top) temperature and tracer fields at day 15 and (bottom) along-isobath component of velocity (v) across the slope. Convergence in the boundary layer and ejection of BBL fluid into the interior change the density field there and subsequently increase the southward interior current.

by tides (Fig. 9). A strong thermocline caps the thin mixed layer. Also, the BBL height at the end of the downwelling phase is the same as in the standard case despite the more vigorous forcing here.

b. Variable interior stratification

In this section, the upper slope is assumed to be stably stratified at one-half of the gradient as in the lower slope. The interior current is constant at -15 cm s^{-1} (see section 2d).

Then, the southward-flowing constant interior current will impose a downslope Ekman flow that is shut down faster on the lower half of the slope. BBL flow convergence around the front and upwelling (Fig. 10a) cause the isotherms in the interior to dome accordingly. Thermal wind balance in the interior,

$$v(z) = V_g + \frac{\beta g}{f}\int_z^{\text{TOP}} [(T - \overline{T})_x - \alpha(T - \overline{T})_z]\, dz, \quad (11)$$

implies that the interior current V_g above the convergence region will accelerate (Fig. 10b) by an amount given from the second term in the right-hand side in Eq. (11). The distortion of the interior density field is caused entirely by BBL dynamics that give rise to convergence within the BBL and detrainment toward the interior. This narrow accelerated interior current (''jet'') occurs exactly above the foot of the front (Fig. 10b) and is 10 km wide across the slope. The jet is vertically coherent and about 2 cm s^{-1} faster than the geostrophic current.

It is shown therefore that the existence of a density front over a constantly sloping bottom (no shelf break) will give rise to a jet in the interior. In the following section an argument will be given for the dynamic similarity of the jet described here to the shelfbreak jet that has been described by several authors (Pickart 2000; Chapman 2000; Fratantoni et al. 2001; Lozier and Gawarkiewicz 2001).

TABLE 1. Cross-slope and along-slope displacements (km) for each model run. Positive values indicate downslope and northward flow, and negative values indicate upslope and southward flow.

	Left of the front		Right of the front		Downslope	
	Downslope	North	Downslope	North	Downslope	North
Standard	8	−8	4	23	4	11
Second cycle	10	−10	−20	100	0	67
Reversed cycle	3	−7	−1	40	3	47
High diffusion	7	−26	−5	30	−2	7
Greater slope	3	−7	0	40	0	20
Tide plus low frequency	5	−9	1.5	5	1.5	0

5. Summary and conclusions

In the first part of the paper, the effect of a time-dependent interior current with zero mean on the BBL around a temperature front was shown to depend primarily on the frequency of the oscillation and in particular on the relation between the period of the oscillation and the spindown time.

A low-frequency forcing that allowed buoyancy to become important in the stratified region of the slope resulted in divergence of the BBL flow around the front and entrainment of interior fluid into the BBL during upwelling Ekman flow. During the second half of the cycle, downwelling Ekman flow in the BBL led to convergence around the front and detrainment of BBL fluid toward the interior. In general during upwelling (downwelling) the flow at the front exhibited lower (upper) slope flow characteristics. The asymmetrical response of the boundary layer to the downwelling and upwelling parts of the flow and the increasing phase shift of the current closer to the bottom were found to be the most important mechanisms that control the BBL dynamics in the vicinity of the front. The front was found to be a site of large positive relative vorticity increase. The entrainment and detrainment zones that occurred at different times of the cycle and at different positions across the boundary (to the left and to the right of the front, respectively) resulted in a net export of BBL fluid toward the interior as pronounced as that of a steady downwelling forcing (as in RW-I).

These results are in good agreement with observational studies by Houghton and Visbeck (1998). They injected dye tracer into the bottom of a front at the Middle Atlantic Bight shelfbreak region and observed its displacement and dispersion for 3 days. The average flow in the stratified region above the BML was 2 cm s^{-1}, generally downslope in agreement with Figs. 4g and 4h. The diapycnal diffusivity that they deduced was 6×10^{-2} cm^2 s^{-1}, although they stressed that variable eddy diffusivity as large as 10 cm^2 s^{-1} was justified for numerical simulations of the BBL flow. Here the vertical eddy diffusivity ranges between 0.08 and 13 cm^2 s^{-1} (Romanou 1999). Last, the observed detrainment velocities were around 4–7($\times 10^{-3}$ cm s^{-1}) whereas here the detrainment or entrainment velocities range between 5×10^{-4} and 5×10^{-3} cm s^{-1}, which can be verified from Figs. 2e–h if one considers $\partial u/\partial x$ for the same times of the cycle.

TABLE 2. Height above bottom that the detrainment of BBL fluid reaches over the first half and the second half cycle of forcing. Position (absolute value) relative to the initial front (km) that tracer is found at the end of a half and the entire forcing cycle.

	Height above bottom (m)		Position (km)	
	First half	Second half	First half	Second half
Standard	15	40	18	6
Second cycle	75	100	15	10
Reversed cycle	30	40	10	8
Greater slope	18	50	15	10
Tide plus low frequency	15	40	18	10

The displacements across and along the slope for the standard and all subsequent model runs are summarized in Table 1. The detrainment of BBL fluid into the interior after a half and a full cycle of forcing for each model run are also summarized in Table 2.

During the second cycle of the same low-frequency forcing, the detrainment around the front was doubled. The net circulation above the lower slope had a stronger northward component and a much reduced downslope component. Relative vorticity was again increased at the front. In general, the second cycle gave a much different picture around the front. The second upwelling phase acted upon a very thick mixed layer produced by the downwelling phase of the first cycle. Only the lower levels of this mixed layer restratified, while the top layers maintained the downwelling character (staircase-like layers).

Increasing the background diffusivity resulted in a reduction of the net northward flow and a reversal of the net cross-slope flow (small upslope flow). Around the front both transports were the same qualitatively but larger in magnitude. The relative vorticity increase was larger.

When the forcing cycle was initiated with a downwelling rather than an upwelling phase, more cold slope water ended up on the upper slope. This cold tongue of slope water to shallower depths implies more transport of nutrients upslope that could be vital for benthic populations there.

Increasing the slope inclination led to larger net northward flow and smaller downslope. Again, the vorticity

input around the front was increased relative to the standard case and the detrainment more vigorous. The intrusion of lower-slope flow to the left of the front was also shown to be more effective and persistent (Romanou 1999). The basic assumption behind this study had been that the far fields in the upper and lower slope regions (i.e., far away from the front) are independent and only interact around the front. However, this case shows that the front affects the flow on the upper slope.

Tidal forcing was shown to have no effect at the front, in agreement with Ramsden (1995), because the tidal period was much less than the spindown time. The buoyancy force did not have time to arrest the Ekman flow and thus no entrainment or detrainment occurred at the front. However, tidal forcing superimposed on a low-frequency current resulted in effects quite different than those of a low-frequency forcing case alone. On the lower slope the net circulation was again downslope but much weaker. Around the front the mean along-slope circulation became more southward before the front and less northward after the front. Because of the presence of the tide, the lower slope maintained some turbulent mixing, even as the forcing decelerated and the intrusion of lower slope flow extended farther to the left of the front. However, the detrainment was not found to be more effective in exporting boundary layer flow towards the interior than the standard case.

Middleton and Ramsden (1996) noted that the cross-slope residual flow on the stratified slope region may be too small relative to other cross-slope flows to be of any importance. However, MacDonald et al. (1999, manuscript submitted to *Mar. Ecol. Prog. Ser.*) found that, for some benthic organisms (sea fans) on the continental slope, the residual across slope flows may be important. While the along-slope flows (both mean and transient) were much stronger than the across-slope flows, the sea fans aligned themselves to capture the downslope effects. In the present work, downslope flow was encountered on the lower slope two out of three times [sections 4a(7), 4a(3), and 4a(4)]. Some current-meter record measurements (Harkema and Weatherly 1996) also show persistent downward flow in a BBL over the slope in a region where the flow above the BBL was variable and predominantly along the isobaths.

The finding of rectified, residual, along-isobath flows and transports in the BBL was unexpected. While the values are sensitive to initial conditions at the start of each cycle, the choice of background diffusivity, and whether tidal effects are included, the rectified flows are large. They typically ranged between 1 and 6 cm s^{-1}, and the associated along-isobath displacements over 23 day tidally modulated cycle dynamically varied by tens of kilometers, sometimes about 100 km. They were due to asymmetries in the cross-slope component of the bottom stress (typically upwelled BBLs are more effectively arrested than downwelled ones) and thermal wind flows generated in the BBL, and tended to be larger around the front. Whether these rectified, along-isobath BBL flows actually exist and, if so, whether they have practical consequences remains to be seen.

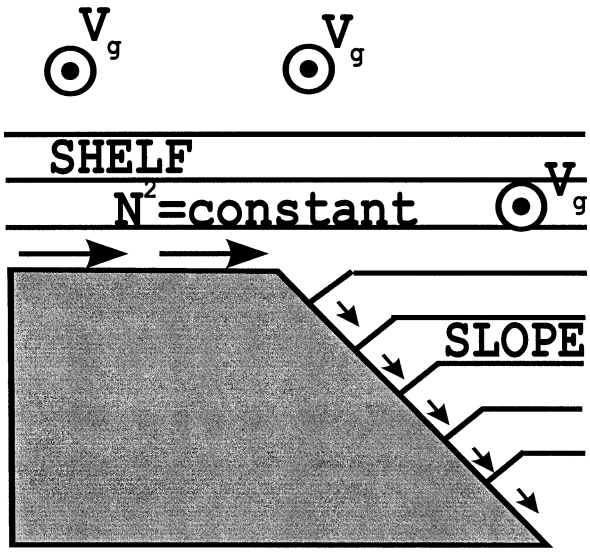

FIG. 11. Schematic representation of the low-frequency forcing case near the shelfbreak: Ekman flow (arrows) over boundary with variable slope and constant stratification N^2. The interior current V_g is time dependent ($T = 23$ days) and flows southward; the Coriolis parameter f is positive. Over the shelf, assumed level, the only effect of $N^2 =$ const is to limit the thickness of the bottom boundary layer (BBL). Otherwise, the BBL stress and transport are as for a BBL formed in a $N^2 = 0$ case. Over the slope, when the bottom slope is assumed fixed, the BBL is a buoyant one as described in Middleton and Ramsden (1996).

The thickness of the BML at different parts of the cycle was found to be different. Therefore, the existence of even a slight time dependency in the interior current could explain the BML height difference Houghton and Visbeck (1998) encountered within the Middle Atlantic Bight during the two cruises (3–6 and 10–12 m).

As a sensitivity check some of the runs were recomputed on a finer horizontal resolution ($\delta x = 500$ m) and a smaller time step ($\delta t = 1$ min). Although there were some small quantitative changes (e.g., the net downslope transport in the lower slope for the standard case increased from 4×10^4 to 5×10^4 cm^2 s^{-1}), the same qualitative behavior described here was repeated and the results were slightly smoother in the downslope region.

Last and as in RW-I, the results found here may be extended to the area of the continental shelf break where there is a discontinuity in the slope rather than the stratification (Fig. 11). It has been argued in RW-I that the buoyancy term in the cross-slope momentum balance, that is, $g\beta\alpha(T - \overline{T})$, describes the front dynamics (when T varies with x) or, equally well, the variable topography dynamics (when α varies with x). In other words, the case of a constant bottom slope and variable stratification (front) is dynamically similar to the case of a variable bottom slope (as in the shelf break) and uniform background stratification. Therefore, alternating phases of mixed layer growth and collapse, detrainment and en-

trainment around the slope discontinuity, and bottom stress variation are expected around the continental shelf break in similar fashion as to the ones around the front. Indeed, Yanagi et al. (1992) measured large vertical sediment fluxes occurring during the ebb rather than during the flood tides at the Tokyo Bay shelf break. They also suggested that this ''tidal pump'' was a result of the differential turbulent mixing and water depth across the sides of the shelf edge. The semidiurnal tide was very strong and the tidal ellipse was mainly aligned with the north–south direction, that is, along the slope, in accordance with the results presented here. Also, in Puig et al. (2001) it is nicely shown that the shelfbreak is a region of detaching bottom layers. However, it is not clear what the interior flow was like then.

In this light, using the results of section 4b, one can explain the shelfbreak jet that several investigators have described observationally and numerically. It was shown there that the BBL convergence at the foot of the front (imposed by a southward interior current) will result in doming of the isopycnals in the interior and therefore, because of thermal wind balance, acceleration southward of the interior current. The southward jet is the result of the front and shutdown buoyant Ekman layer dynamics and is independent of the existence of a shelf break. However, in the dynamically similar scenario described in the previous paragraph, one will expect to see a southward jet also when the background stratification is constant but the bottom topography varies as near the shelf break. Therefore, an along-isobath jet is the result of BBL dynamics related to the shutdown of the cross-slope Ekman flow that can arise because of either variable background stratification or variable topography (or of course both). All investigators agree that the jet speed is about 10–50 cm s^{-1} with much of the variability attributed to local wind forcing, circulation of the slope water and Gulf Stream rings, and the effect of tidal forcing (Fratantoni et al. 2001). The current found here is 16 cm s^{-1}.

Acknowledgments. We thank Dr. Aike Beckmann and Dr. Harold Mofjeld for insightful discussions. Financial support of this work was provided by the Department of Energy (Grant DE-FG05-92ER61416) and the National Science Foundation (Grant OCE-92-06117).

REFERENCES

Chapman, D. C., 2000: Boundary layer control of buoyant coastal currents and the establishment of a shelfbreak front. *J. Phys. Oceanogr.,* **30,** 2941–2955.

——, and S. J. Lentz, 1994: Trapping of a coastal density front by the bottom boundary layer. *J. Phys. Oceanogr.,* **24,** 1464–1479.

Dietrich, D., 1993: Sandia Ocean Modeling System. Sandia National Laboratories Contractor Report, Albuquerque, NM, 56 pp.

——, M. G. Marietta, and P. J. Roache, 1987: An ocean modeling system with turbulent boundary layers and topography: Numerical description. *Int. J. Numer. Methods Fluids,* **7,** 833–855.

Fratantoni, P. S., R. S. Pickart, D. J. Torres, and A. Scotti, 2001: Mean structure and dynamics of the shelfbreak jet in the Middle Atlantic Bight during fall and winter. *J. Phys. Oceanogr.,* **31,** 2135–2156.

Gawarkiewicz, G., and D. C. Chapman, 1992: The role of stratification in the formation and maintenance of shelf-break fronts. *J. Phys. Oceanogr.,* **22,** 753–772.

Harkema, R., and G. L. Weatherly, 1996: A compilation of moored current meter data from the western boundary of the Brazil Basin for the Deep Basin Experiment, Sept. 1993–March 1995. Dept. of Oceanography Tech. Rep. C.M.F.-96-01, Florida State University, Tallahassee, FL, 72 pp. [Available online at http://ocean.fsu.edu/georges/cmf/brbamain.htm.]

Houghton, R. W., and M. Visbeck, 1998: Upwelling and convergence in the Middle Atlantic Bight shelfbreak front. *Geophys. Res. Lett.,* **25,** 2765–2768.

Kim, Y.-Y., G. L. Weatherly, and L. J. Pietrafesa, 2001: On the mass and salt budgets for a region of the continental shelf in the southern Mid-Atlantic Bight. *J. Geophys. Res.,* **106** (C12), 31 263–31 282.

Lentz, S. J., and J. H. Trowbridge, 1991: The bottom boundary layer over the northern California shelf. *J. Phys. Oceanogr.,* **21,** 1186–1201.

Lozier, M. S., and G. Gawarkiewicz, 2001: Cross-frontal exchange in the Middle Atlantic Bight as evidenced by surface drifters. *J. Phys. Oceanogr.,* **31,** 2498–2510.

McCready, P., and P. Rhines, 1993: Slippery bottom boundary layers on a slope. *J. Phys. Oceanogr.,* **23,** 5–22.

Mclean, A. R., and J. Yean, 1987: Velocity and stress in the deep-ocean boundary layer. *J. Phys. Oceanogr.,* **17,** 1356–1366.

Mellor, G., and T. Yamada, 1982: Development of a turbulence closure model for geophysical fluid problems. *Rev. Geophys. Space Phys.,* **20,** 851–875.

Middleton, J., and D. Ramsden, 1996: The evolution of the bottom boundary layer on the sloping continental shelf: A numerical study. *J. Geophys. Res.,* **101** (C8), 18 061–18 077.

Pickart, R. S., 2000: Bottom boundary layer structure and detachment in the shelfbreak jet of the Middle Atlantic Bight. *J. Phys. Oceanogr.,* **30,** 2668–2686.

Puig, P., J. B. Company, F. Sarda, and A. Palanques, 2001: Response of deep-water shrimp populations to intermediate nepheloid layer detachments on the northwestern Mediterranean continental margin. *Deep-Sea Res.,* **48,** 2195–2208.

Ramsden, D., 1995: Response of an oceanic bottom boundary layer on a slope to interior flow. Part II: Time-dependent interior flow. *J. Phys. Oceanogr.,* **25,** 1688–1695.

Richards, K. J., 1982: Modeling the benthic boundary layer. *J. Phys. Oceanogr.,* **12,** 428–439.

Romanou, A., 1999: Buoyant Ekman layers over variable topography. Ph.D. dissertation, Florida State University, 144 pp.

——, and G. L. Weatherly, 2001: Numerical simulations of buoyant Ekman layers in the presence of variable stratification. Part I: Constant interior forcing. *J. Phys. Oceanogr.,* **31,** 3096–3120.

Weatherly, G. L., 1975: A numerical study of time-dependent turbulent Ekman layers over horizontal and sloping bottoms. *J. Phys. Oceanogr.,* **5,** 288–299.

——, and P. J. Martin, 1978: On the structure and dynamics of the oceanic bottom boundary layer. *J. Phys. Oceanogr.,* **8,** 557–570.

——, S. L. Blumsack, and A. A. Bird, 1980: On the effect of diurnal tidal currents in determining the thickness of the turbulent Ekman bottom boundary layer. *J. Phys. Oceanogr.,* **8,** 297–300.

Yamada, T., 1979: An application of a three-dimensional, simplified second-moment closure numerical model to study atmospheric effects of a large cooling-pond. *Atmos. Environ.,* **13,** 693–704.

Yanagi, T., M. Shimizu, T. Saino, and T. Ishimaru, 1992: Tidal pump at the shelf edge. *J. Oceanogr.,* **48,** 13–21.

Yankofsky, A. E., and D. C. Chapman, 1997: A simple theory for the fate of buoyant coastal discharges. *J. Phys. Oceanogr.,* **27,** 1386–1401.